

Communication

# A High Precision Fiber Optic Fabry–Perot Pressure Sensor Based on AB Epoxy Adhesive Film

Yanan Zhang <sup>1,2</sup> , Shubin Zhang <sup>1,2</sup>, Haitao Gao <sup>1,2</sup> , Danping Xu <sup>1,2</sup>, Zhuozhen Gao <sup>1,2</sup>, Zheyu Hou <sup>1,2</sup>, Jian Shen <sup>1,2,\*</sup> and Chaoyang Li <sup>1,2</sup>

<sup>1</sup> School of Information and Communication Engineering, Hainan University, Haikou 570228, China; zhangyanan@hainanu.edu.cn (Y.Z.); zhangshb28@mail2.sysu.edu.cn (S.Z.); gaohaitao@hainanu.edu.cn (H.G.); xudanping@hainanu.edu.cn (D.X.); gaozhuozhen@hainanu.edu.cn (Z.G.); houzhayu@hainanu.edu.cn (Z.H.); lichao yang@hainanu.edu.cn (C.L.)

<sup>2</sup> State Key Laboratory of Marine Resource Utilization in South China Sea, Hainan University, Haikou 570228, China

\* Correspondence: shenjian@hainanu.edu.cn

**Abstract:** This paper proposes a Fabry–Perot pressure sensor based on AB epoxy adhesive with ultra-high sensitivity under low pressure. Fabry–Perot interference, located between single-mode fiber (SMF) and hollow-core fiber (HCF), is an ultra-thin AB epoxy film formed by capillary action. Then the thick HCF was used to fix the HCF and SMF at both ends with AB epoxy adhesive. Experimental results show that when the thickness of AB epoxy film is 8.74  $\mu\text{m}$ , and the cavity length is 30  $\mu\text{m}$ , the sensor has the highest sensitivity. The sensitivity is 257.79 nm/MPa within the pressure range of 0–70 kPa. It also investigated the influence of the curing time of AB epoxy on the interference spectrum. Experiments showed that the interference spectrum peak is blue-shifted with the increase of curing time. Our study also demonstrated the humidity stability of this pressure sensor. These characteristics mean that our sensor has potential applications in the biomedical field and ocean exploration.



**Citation:** Zhang, Y.; Zhang, S.; Gao, H.; Xu, D.; Gao, Z.; Hou, Z.; Shen, J.; Li, C. A High Precision Fiber Optic Fabry–Perot Pressure Sensor Based on AB Epoxy Adhesive Film. *Photonics* **2021**, *8*, 581. <https://doi.org/10.3390/photonics8120581>

Received: 7 November 2021

Accepted: 13 December 2021

Published: 16 December 2021

**Publisher's Note:** MDPI stays neutral with regard to jurisdictional claims in published maps and institutional affiliations.



**Copyright:** © 2021 by the authors. Licensee MDPI, Basel, Switzerland. This article is an open access article distributed under the terms and conditions of the Creative Commons Attribution (CC BY) license (<https://creativecommons.org/licenses/by/4.0/>).

**Keywords:** optical fiber sensor; AB epoxy adhesive; thin films; pressure sensor

## 1. Introduction

In recent years, Fabry–Perot (FP) sensors have drawn attention due to many outstanding advantages, such as high sensitivity, small size, high measurement accuracy, high resolution, and extensive dynamic range [1–6]. Compared with traditional electronic sensors, optical fiber pressure sensors have many unique merits, such as having the advantages of lateral strain insensitive and minimal temperature crosstalk [7–11]. At present, due to the characteristics mentioned above, optical fiber pressure sensors are widely used in many fields such as biomedical testing, environmental monitoring, ocean exploration, and so on [12–16]. For that reason, improving pressure sensitivity and simplifying the fabrication process has always been a significant concern in this field.

In 1987, Beheim, G. et al. proposed the diaphragm-type non-intrinsic FP fiber sensor for the first time. The optical fiber FP cavity mainly demonstrates three representative structures: intrinsic, non-intrinsic, and linear composite cavity [17]. More and more high sensors have been developed that use different materials to form an FP cavity [18–22]. They have the advantage of FP cavity length and can be designed and adjusted artificially according to requirements; in this way, the cavity length can be precisely controlled, and the cavity length can be adjusted flexibly. In 2018, [23] Wang et al. proposed a miniature pressure sensor with a coaxial air cavity. The sensitivity is 193 pm/MPa within the pressure measurement range of 0–1 MPa. Nevertheless, they require a complicated manufacturing process and are not sensitive enough. In 2019, [24] Ricardo, G. et al. demonstrated that the sensitivity of FP cavities could be improved by adding resin layers around the FP

cavities between fiber tips. The hydrostatic pressure sensitivity can reach 475 pm/MPa, and the working range is much larger (in the order of MPa). Luo et al. [25] reduced the thickness of the optimized PDMS film to 20  $\mu\text{m}$ , and the sensitivity of the optical fiber pressure sensor could reach 100 pm/MPa. However, the sensitivity is not large enough. In 2020, Zhang et al. [26]. prepared micron-scale all-silicon films by improving the pressure-assisted discharge method. When the external air pressure was between 100 and 1600 kPa, the sensitivity of the FP cavity was 6790 pm/MPa. The sensor has the advantages of the working range being much more extensive and low cost; however, the process is very complicated, and the sensitivity is not large enough. We consider selecting a new material to form the FP cavity based on the above characteristics. AB epoxy adhesive is one specific epoxy adhesive that has good electrical and mechanical performance after the curing process, such as good insulation, compression resistance, and high adhesive strength. Therefore, the AB epoxy (AWG97033) is selected as the material of the pressure-sensitive film.

Our work mainly studied the sensitivity measurement of fiber optic pressure sensors under low-pressure conditions. When the pressure range was 0–70 kPa, the maximum pressure sensitivity was 257.79 nm/MPa. The advantages of this sensor over other similar high-precision sensors are mainly the increase in sensitivity and the simpler production process. The particular structure based on the sensor can be applied to biological penetration detection and has some potential applications for marine engineering.

## 2. Fabrication and Principle

The pressure sensor based on AB epoxy adhesive film is mainly composed of single-mode optical fiber (SMF, Corning SMF28 e+), hollow-core fiber (HCF, TSP075150, with a core diameter of 75  $\mu\text{m}$  and a cladding diameter of 150  $\mu\text{m}$ ), AB epoxy adhesive, thick HCF (TSP150375, with a core diameter of 150  $\mu\text{m}$  and a cladding diameter of 363  $\mu\text{m}$ ), etc. Figure 1 shows the schematic diagram of the sensing structure. The AB epoxy film is formed in the HCF, the SMF and HCF with the film are fixed in the thick HCF.

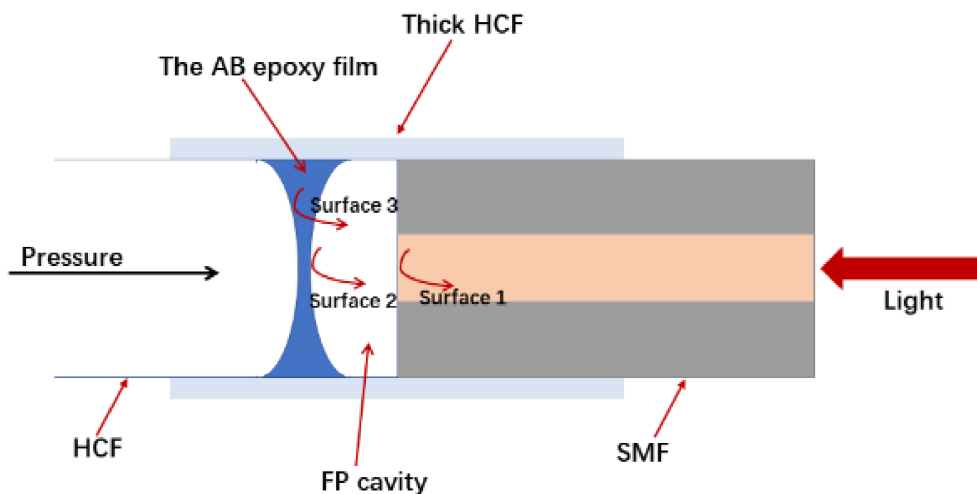


Figure 1. Schematic diagram of the sensing structure.

There are three reflective surfaces: Surface 1, Surface 2, and Surface 3 [27]. When the light is coupled to the core of the SMF, it encounters the first reflection surface 1 (the end face of the SMF) and the second reflection Surface 2 (inside the AB epoxy film) after passing through the FP cavity. Light passes through the AB epoxy film to reach the third reflective Surface 3 (outside of the AB epoxy film) on the far end surface, and the beams of the three reflecting surfaces form the interference phenomenon.

The reflected light intensity can be expressed by the formula [12]:

$$I = |E|^2 = \left| E_1 - E_2 \exp\left(\frac{4\pi}{\lambda} \eta_{air} L\right) + E_3 \exp\left[\frac{4\pi}{\lambda} (\eta_{AB} t + \eta_{air} L)\right] \right|^2 \tag{1}$$

where  $L$  is the length of the FP cavity,  $t$  is the thickness of the AB epoxy film. The refractive index of the core is  $\eta_{core} = 1.4492$ , and the refractive index of the AB epoxy adhesive film is  $\eta_{AB} = 1.554$ . The FP cavity is filled with air, the refractive index of air is  $\eta_{air} = 1$ .

Expand the Formula (1) to get:

$$I = \underbrace{E_1^2 + E_2^2 + E_3^2}_A - \underbrace{2E_1E_2 \cos\left(\frac{4\pi}{\lambda} \eta_{air} L\right)}_B - \underbrace{2E_2E_3 \cos\left(\frac{4\pi}{\lambda} \eta_{AB} t\right)}_C + \underbrace{E_1E_3 \cos\left[\frac{4\pi}{\lambda} (\eta_{AB} t + \eta_{air} L)\right]}_D \tag{2}$$

In Formulas (1) and (2),  $E_1, E_2$  and  $E_3$  are the amplitudes of the three reflected waves of Surface 1, Surface 2, and Surface 3, respectively, and  $\lambda$  is the light wavelength. From the above formula, we can see that the light intensity is mainly composed of four parts: A, B, C, and D. Those three reflected waves interact with each other and form an interference spectrum, which is related to the thickness  $t$  of the AB epoxy adhesive film and the cavity length  $L$ . The resonance peak position of the three-beam interference spectrum depends on the three parts B, C, and D in Formula (2). The part B is the interference of the FP cavity, and affected by the cavity length is  $L$ ; the part C is the interference effect of the film itself, and influenced by the thickness of the film is  $t$ ; part D is the interference caused by the combined action of the FP cavity and the reflective film.

In this experiment, because the thickness of the AB epoxy film is very thin, considering the limit case, when  $t \rightarrow 0, \eta_{AB} t \rightarrow 0$ , the Formula (2) can be written as:

$$I \approx E_1^2 + E_2^2 + E_3^2 - 2(E_1E_2 - E_1E_3) \cos\left(\frac{4\pi}{\lambda} \eta_{air} L\right) - 2E_2E_3 \cos\left(\frac{4\pi}{\lambda} \eta_{AB} t\right) \tag{3}$$

When  $t \rightarrow 0$ , the three-beam interference will gradually evolve into two-beam interference, and the interference spectrum is shown in Formula (3).

When external pressure is loaded, due to the pressure difference between the inside and outside of the sealed air cavity, the AB epoxy adhesive ultra-thin film layer is elastically deformed, which in turn changes the length of the Fabry–Perot interference (FPI) cavity, causing the corresponding interference spectrum to shift. The amount of deformation  $\Delta L$  is the variation of FP cavity length, and it can be expressed by the following formula [28]:

$$\Delta L = \frac{3(1 - \nu^2)P}{16Et^3} r^4 \tag{4}$$

where  $\nu$  is the Poisson’s ratio of the film,  $r$  is the effective radius of the film,  $E$  represents Young’s modulus of the film,  $t$  is the thickness of the film,  $P$  is the change of pressure difference between inside and outside the diaphragm. Since the magnitude of the deformation of the AB epoxy film has a decisive influence on the sensitivity of the sensor, the air pressure response sensitivity  $S$  can be expressed as:

$$S = \frac{3(1 - \nu^2)}{16Et^3} r^4 \tag{5}$$

The core unit of the thin-film Fabry–Perot fiber-optic pressure sensor is a pressure-sensitive thin film, which undergoes elastic deformation due to the pressure difference between the inside and outside of the sealed air cavity. When the external pressure changes, the cavity length of the interference cavity changes. Figure 2 shows the influence of pressure on the deformation of type AB epoxy film simulated by ANSYS. Figure 2a is the simulation diagram made at 5000 Pa. The black line displayed the state of the film when the external air pressure was not initially loaded. When the external air pressure is increased,

a significant deformation is observed, which leads to the change of the length of the FP cavity. According to Formula (4) and the study of pressure-induced material birefringence in capillary fibers [29], it can be predicted that the variation of the FP cavity lengthened linearly with pressure variation. Figure 2b shows the deformation of the diaphragm for different pressure values. It was found that the linearity was 95.524%. There was a linear relationship, which is consistent with the theoretical results. In the experiment, it was found that the linearity disappeared when the pressure was more than 70 kPa, so the range of linearity of the membrane deformation was from 0 to 70 kPa.

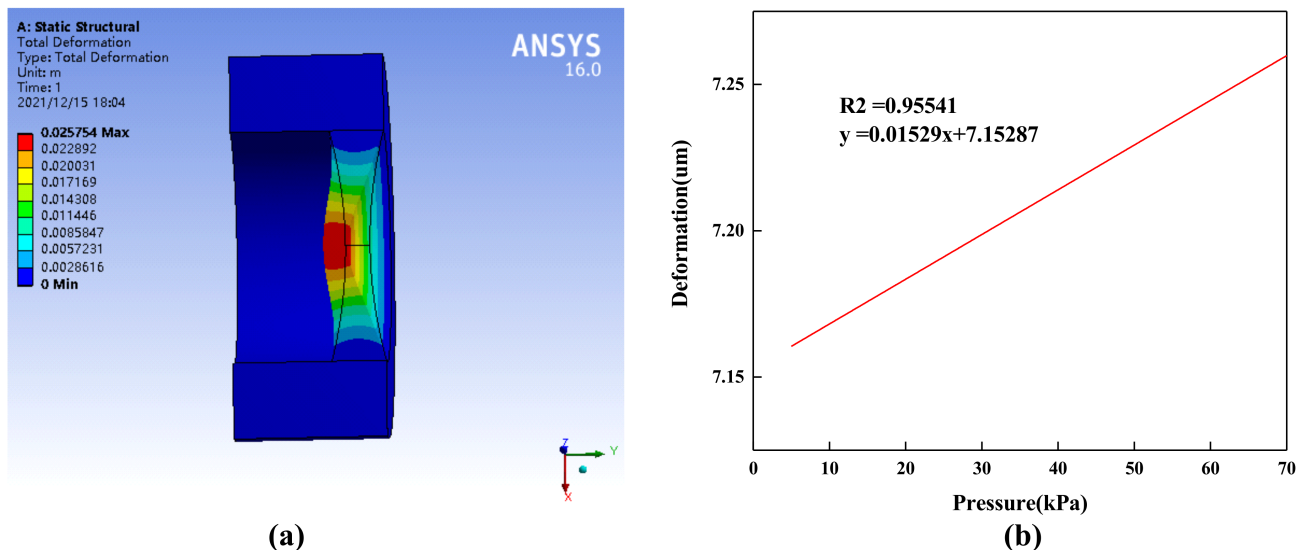


**Figure 2.** Stress and deformation of thin-film at external air pressure: (a) Simulation diagram made at 5000 Pa; (b) Deformation of the diaphragm for different pressure values.

For our FP pressure sensor, the preparation process of the AB epoxy film is particularly important. The process is shown in Figure 3. Firstly, adhesive A and adhesive B were mixed at a volume ratio of 1:1. Secondly, the SMF was inserted vertically into the mixed AB epoxy adhesive. Due to the capillary action, the SMF dipped a certain amount of AB epoxy adhesive. The SMF with the AB epoxy adhesive film and cut HCF were placed at both sides of the optical fiber fusion splicer (80C+, Fujimura Co., Ltd., Tokyo, Japan). The SMF and HCF were accurately contacted by an optical fiber fusion splicer so that the AB epoxy film was transferred to the HCF due to capillary action. Then an SMF with the amplified spontaneous emission (ASE, the KG-ASE series of Beijing Kangguan Century Optoelectronics Technology Co., Ltd., Beijing, China) was connected to the HCF with the AB epoxy film by fusion splicer.

It was found that the time of dipping in the liquid affected the amount of AB epoxy entering the HCF and the length of the cavity. The longer the time, the shorter the FP cavity will be. In order to get repeatable results, the time of dipping in AB epoxy adhesive should be strictly controlled [30].

Figure 4 shows the spectrum of reflective light intensity obtained at different curing times. Figure 4a reveals that the reflected range changed the curing time of AB epoxy adhesive. From the red dot-line box, it can be found that the interference spectrum underwent a blue shift. The shift of the spectrum gradually decreased and finally stabilized. When curing time reached 30 min, the interference spectrum became stable. Figure 4b shows the dependence of the peak position of the interference spectrum on the curing time. It can be seen that the range showed an inverse proportional function curve as the curing time increased, and it became stable when the curing time was about 30 min. Thus, the curing time of the AB epoxy adhesive was about 30 min, and the adhesive could meet the requirements of the experiment.

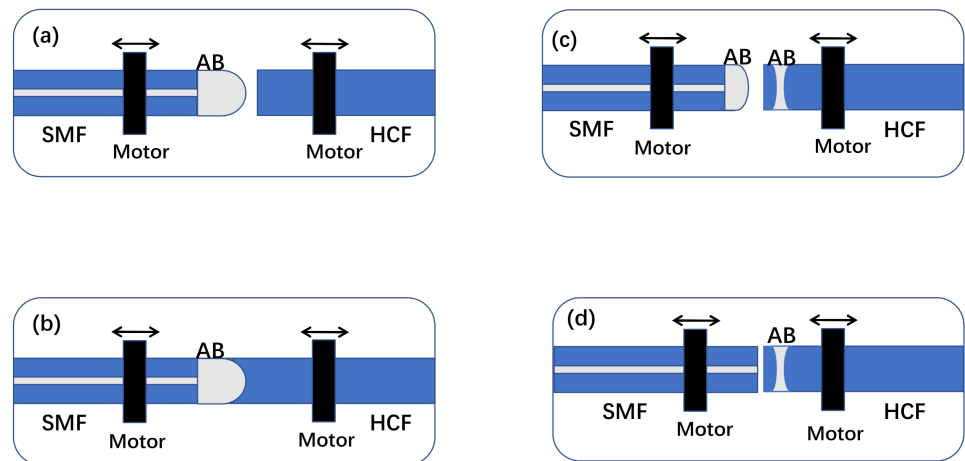


**Figure 3.** Flow chart of sensors structure preparation: (a) the SMF with the AB epoxy adhesive film and cut HCF are placed at both sides of the optical fiber fusion splicer; (b) the SMF and HCF are accurately contacted by optical fiber fusion splicer; (c) the AB epoxy film is transferred to the HCF due to capillary action; (d) the SMF with the ASE is connected the HCF with the AB epoxy film by fusion splicer.

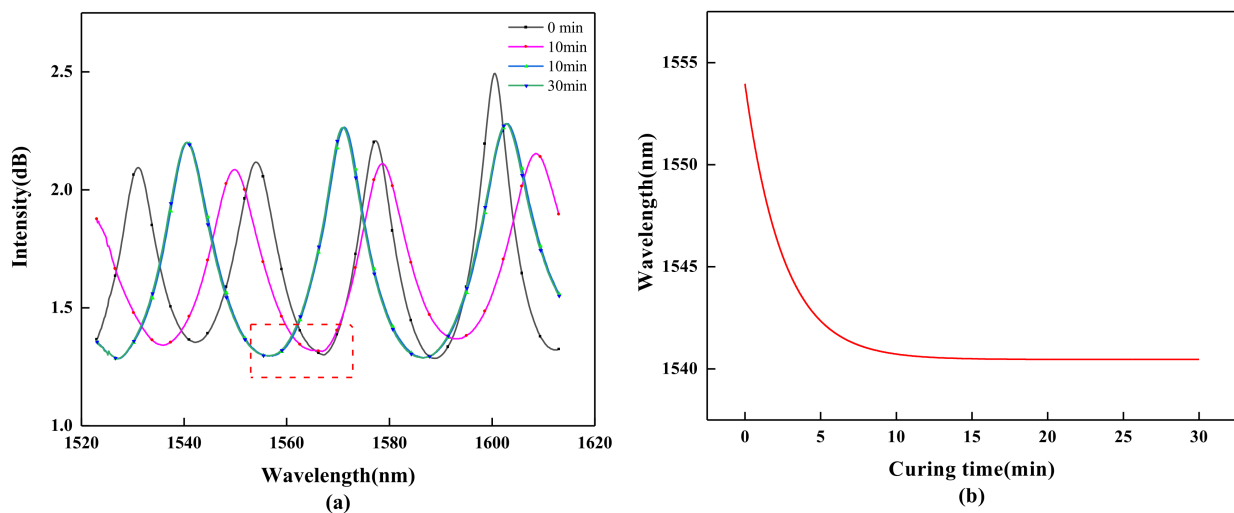


**Figure 4.** AB adhesive curing time spectrum: (a) Reflected spectrum at different curing times; (b) Fitting image of curing time.

After the AB epoxy adhesive film was cured, the SMF and the HCF with the film were inserted into a section of thick HCF (2 cm long, 363  $\mu\text{m}$  outer diameter, and 150  $\mu\text{m}$  inner diameter) from both sides. The distance between the two SMF and HCF was monitored in real-time by the microscope control platform so that the length of the interference cavity could be precisely controlled, and an interference micro-cavity with a cavity length of 30  $\mu\text{m}$  was obtained. Furthermore, the AB epoxy adhesive was used to fix the two ends of the thick HCF on the SMF and HCF to ensure the stability of the whole structure. The packaged system is shown in Figure 5. The design inside the dotted line in Figure 5 corresponds to Figure 1 schematic diagram of the sensing structure.

The cavity length and the thickness of the AB epoxy film are difficult to measure directly; however, there is an indirect way to determine their size. The outer diameter of SMF used is 125  $\mu\text{m}$ , and the length of the cavity and the thickness of AB epoxy film can be approximated by scale transformation [31]. Figure 6 is the camera picture of cavity length and AB epoxy film thickness. Taking the outer diameter of SMF as the reference, the cavity

length  $L$  was measured as  $30.35\ \mu\text{m}$ , and the thickness  $t$  of the AB epoxy adhesive film was  $8.74\ \mu\text{m}$ .

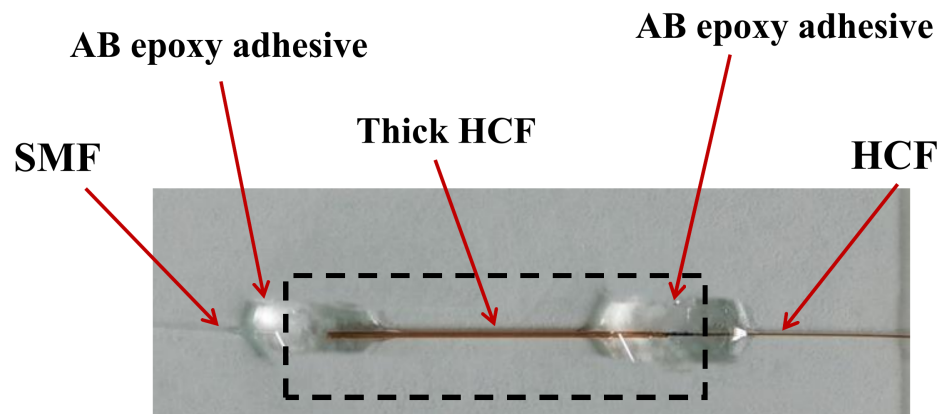


**Figure 5.** The picture of the packaged sensor structure.

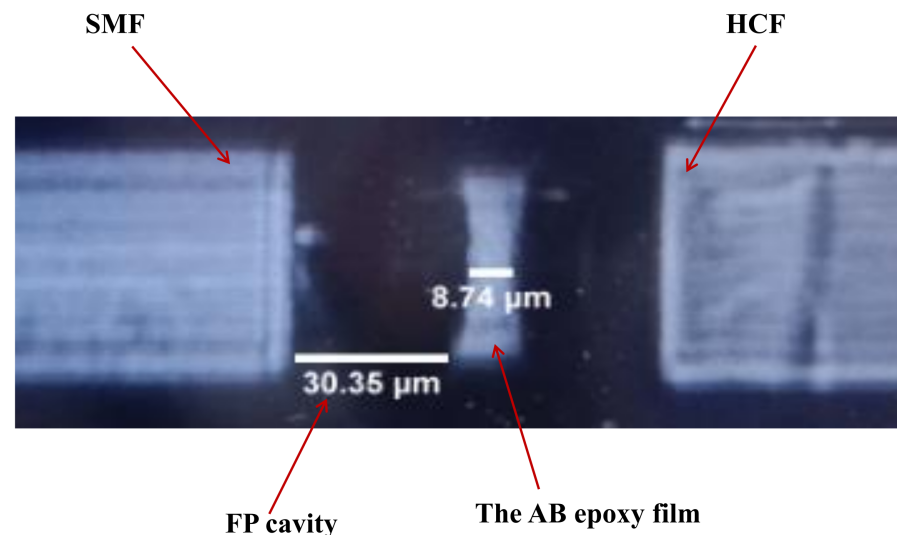


**Figure 6.** The picture of cavity length and film thickness marking.

### 3. Testing and Analysis

The experimental test schematic diagram is shown in Figure 7. The instruments in the analysis system included a high-precision pressure gauge pump, fiber optic circulator, ASE, and optical spectrum analyzer (OSA). The wavelength range of the ASE light source was from 1530 to 1610 nm. The desktop air pump adopted the Const 162 series of Beijing Const Instrument Technology Co., Ltd. Pressure pumps and high-precision pressure meters provided and calibrated pressure changes. In this way, we could provide a linearly varying pressure value with a resolution of 10 Pa. OSA adopts Yokogawa's AQ6370D, which could be used to observe and record the spectrum changes in the range of 600 to 1750 nm; the spectrum measurement range was 600–1750 nm. The minimum measurement resolution was 30 pm.

In Luo's work [25], the influence of the FP cavity length on the sensor's sensitivity was described in detail, which proves that the longer the cavity length, the lower the sensor sensitivity. Our work showed that the sensitivity of the sensor structure was mainly related to the size of the FP cavity and the thickness of the AB epoxy film. In order to study the impact of AB epoxy film on sensor sensitivity, it was necessary to fix the FP cavity length (the cavity length range is about  $30\ \mu\text{m}$ ). It can be seen from Formulas (2)–(5) that the FP pressure sensitivity was inversely proportional to the thickness of the film. That is, the thinner the film, the higher the pressure sensitivity.

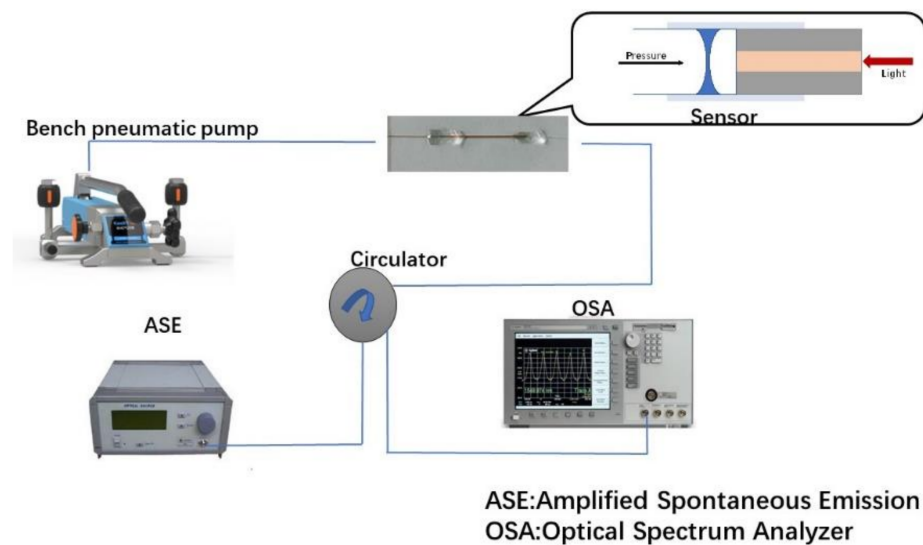


**Figure 7.** Schematic diagram of experimental test.

Table 1 shows the comparison chart of pressure and sensitivity with the cavity length fixed at 30  $\mu\text{m}$  and different film thicknesses. From the comparative sensitivity of the sensor shown in Table 1, we know that, as the thickness of the AB epoxy film increased, the sensitivity became lower, which is consistent with the conclusion of the Formulas (2)–(5).

**Table 1.** Comparison table of pressure and sensitivity under different AB epoxy film thicknesses.

| Thickness   | 7.96 $\mu\text{m}$ | 7.46 $\mu\text{m}$ | 7.10 $\mu\text{m}$ |
|-------------|--------------------|--------------------|--------------------|
| Pressure    | 0–50 kPa           | 0–10 kPa           | 0–8 kPa            |
| Sensitivity | 63.36 nm/MPa       | 297 nm/MPa         | 331.2 nm/MPa       |

Figure 8 shows the movement of the interference spectrum peak for the different film thicknesses in Table 1 at the same pressure. The abscissa is the wavelength, and the vertical is the interference intensity. It was found that the influence spectrum underwent a blue shift as the film thickness decreased. It also showed that the interference spectrum underwent a blue shift as the curing time increased. The same spectra movement is obtained from Figure 4. It can be speculated that the thickness of the AB epoxy film will become thinner as the curing time increases.

Through experiments, it can be found that a thinner film layer is not necessarily better. Under capillary action, if the film layer is too thin, it will cause the AB epoxy adhesive to have a significant diffusion distance at low viscosity, and the formed film layer has a more considerable curvature. It is impossible to form an FP cavity in the end.

Experiments showed that when the thickness of AB epoxy film was less than 7  $\mu\text{m}$ , a slight change of the external air pressure would bring a vast deformation to the AB epoxy film and it would eventually break. In subsequent experiments, when the film thickness was 8.74  $\mu\text{m}$ , the pressure could be measured in the range of 0–70 kPa; however, when the film thickness was 7.10  $\mu\text{m}$ , the maximum pressure was 8 kPa. In our experiment, to get an extensive working range (0–70 kPa) with relatively high sensitivity (257.79 nm/MPa), the film thickness of 8.74  $\mu\text{m}$  was selected as the sensing unit.

By precisely adjusting the air pressure of the desktop air pump, the spectrum could be monitored and recorded by the spectrometer. Figure 9 shows the interference spectrum measured by the sensor in the range of 0 to 70 kPa. In an experiment, taking the 10 kPa as a step, the scope was calculated after each loaded pressure measurement point was maintained for 30 s to ensure the stability of the measurement data. From Figure 9a, it can be observed that there were three interference peaks in the wavelength range of 1530–1605 nm. Figure 9b shows the local enlargement of one interference spectrum. By

selecting the peak position of the interference peak near the 1565 nm wavelength to track the wavelength shift, the relationship curve between the external air pressure and the wavelength shift is obtained. With the increase of air pressure, the peak of the interference spectrum has a blue shift.

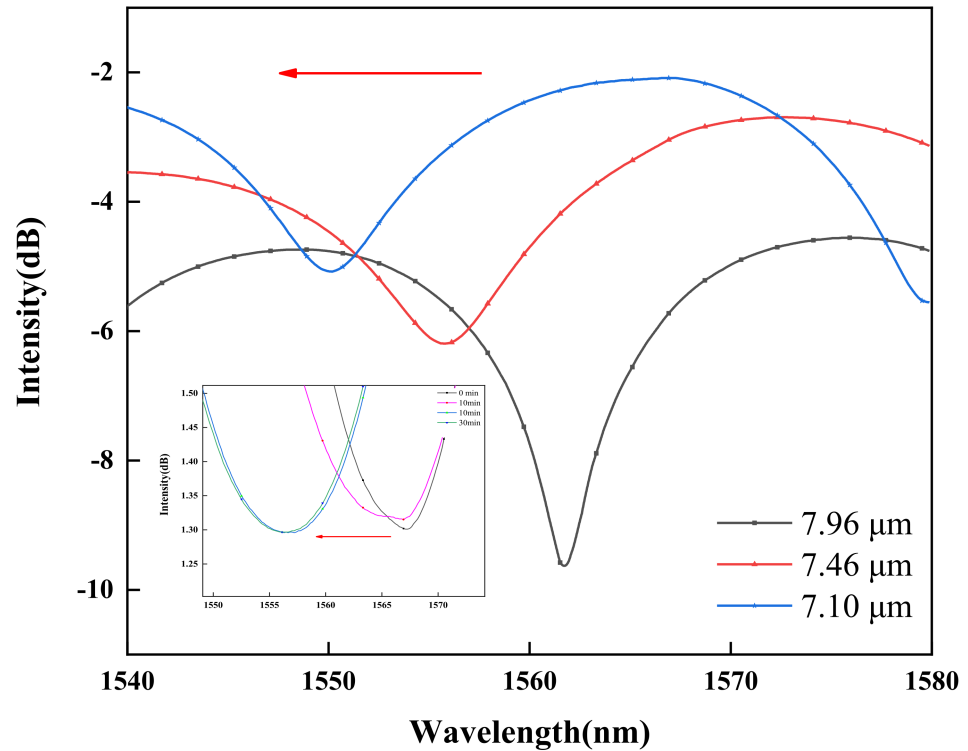


Figure 8. The movement of the interference spectrum peak for different film thicknesses and curing time at the same pressure.

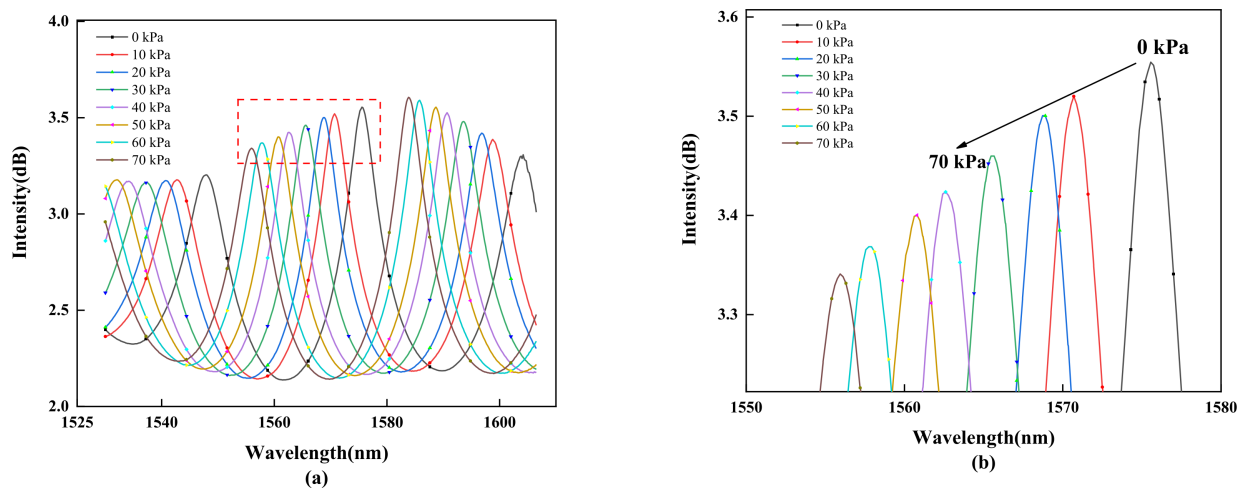


Figure 9. Interference spectrum movement under pressure change of 0–70 kPa: (a) interference spectra at the 75 nm band; and (b) local enlargement of one interference spectrum.

Figure 10 shows the schematic diagram of the wavelength and intensity shift of the central interference peak of the sensor under pressure changes. By wavelength demodulation, the calculated sensitivity of the sensor was 257.79 nm/MPa, and good linearity of 98.94% was obtained. When intensity demodulation was used, the sensor’s sensitivity was

1.42 dB/MPa, and the linearity was 96.223%. It can be found that it could not only be used for intensity demodulation, but also for wavelength demodulation.

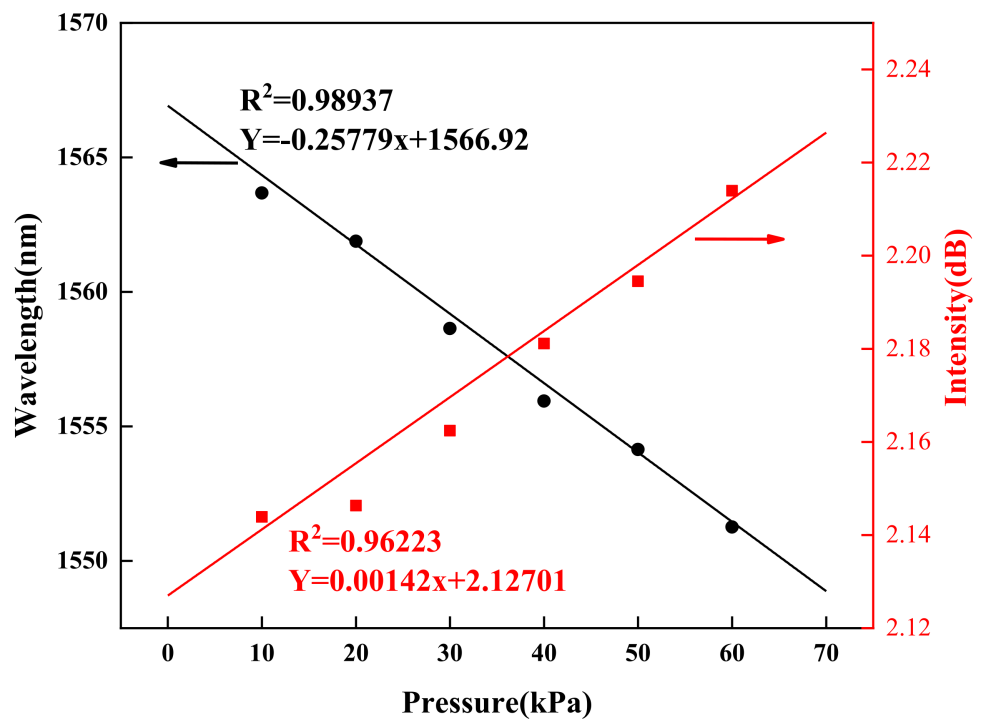


Figure 10. Wavelength and intensity shift with gas pressure.

Sensor resolution is the ability of a sensor to perceive the smallest change in the measured. We defined the sensor resolution as  $\eta$  [26]:

$$\eta = \frac{m}{\alpha} \tag{6}$$

where  $m$  is the smallest detectable wavelength shift of the reflection spectrum,  $\alpha$  is the sensitivity of a sensor which can be expressed as follows:

$$m = 3\sigma \tag{7}$$

The  $\sigma$  is the standard deviation of the total noise output signal resulting from amplitude noise, thermal noise, and OSA spectrum resolution. In this paper,  $m$  was calculated to be 22.55 pm, and hence the sensor resolution  $\eta$  was 87.474 Pa.

The influence of humidity on the sensor has also been studied. At first, the Testo humidity tester (testo608-H1) was used to detect the environment’s moisture. Second, the interference spectrum of the sensor at different humidity was monitored. Figure 11 shows the movement of the interference spectrum at extra humidity. It can be seen that the interference spectrum showed a blue shift as the humidity increased. When the wavelength was between 1520 nm and 1580 nm,  $X_1$ ,  $X_2$ , and  $X_3$  were the trough of wavelength with different humidity (55%, 65%, 75%), respectively. It was found that the offsets were 0.54 nm and 1.44 nm, respectively. It can be speculated that, in a specific range of humidity changes, humidity has a minor influence on our sensor.

This work presents a Fabry–Perot pressure sensor using AB epoxy as the pressure-sensitive film. Table 2 compares the sensitivity of pressure sensors with similar structures in recent years. Reference [12] demonstrate a sub-micron silica diaphragm-based fiber-tip FPI for pressure sensing applications. A high-pressure sensitivity with 1036 pm/MPa in the pressure range of 0 to 2000 kPa. In [26], the thin film of the microbubble was transferred to the end of the single-mode-fiber/glass-tube structure for forming the FPI

cavity. Experimental results show that the sensitivity of this FP cavity was 6790 pm/MPa when the external pressure ranged from 100 to 1600 kPa. However, the production process is complicated. The authors of [27] demonstrated a susceptible gas pressure sensor based on PDMS FPI, with more concise processing steps and lower cost. The pressure sensitivity was 52.173 nm/MPa when the pressure ranged from 100 to 700 kPa. The Fabry–Perot pressure sensor made of AB epoxy adhesive was studied in this paper. The sensor has the characteristics of simple fabrication and high sensitivity. Compared with the recent research, the sensor preparation method in this article has improved the sensor’s sensitivity nearly five times [32–35].

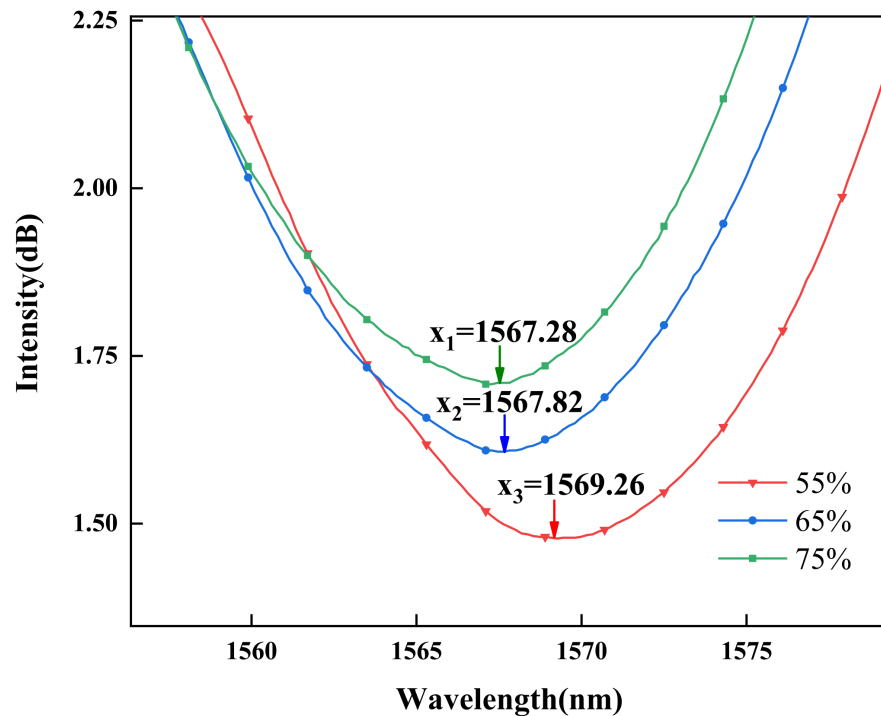


Figure 11. The movement of interference spectra under different humidity conditions.

Table 2. The sensitivity of optical fiber Fabry–Perot pressure sensor.

| Source (Time)  | 2014 [12]         | 2020 [26]            | 2021 [27]     | This paper        |
|----------------|-------------------|----------------------|---------------|-------------------|
| Materials      | sub-micron silica | silicon microbubbles | PDMS          | AB epoxy adhesive |
| Pressure range | 0–2000 kPa        | 100–1600 kPa         | 100–700 kPa   | 10–70 kPa         |
| Sensitivity    | 1036 pm/MPa       | 6790 pm/MPa          | 52.143 nm/MPa | 257.79 nm/MPa     |

#### 4. Conclusions

This work proposes a pressure sensor with ultra-high sensitivity at low pressure based on the AB epoxy film. When the thickness of AB epoxy film was 8.74 μm, and the cavity length was 30 μm, the sensor’s sensitivity was up to 257.79 nm/MPa at the range of 0–70 kPa.

The AB epoxy film became thinner to a certain extent during the curing process, which lead to the blue shift of the interference spectrum. When the curing time was 30 min, the interference spectrum became stable, thus providing reliable support to the structure. The experiment also studied the influence of humidity on sensor performance, the results of which showed that the sensor had good stability when the humidity was between 55% to 75%. However currently, our experiments are somewhat limited and confined to the case where the temperature was stable and constant.

In summary, the optical fiber FP pressure sensor based on AB epoxy adhesive film has the characteristics of high sensitivity at low pressure and good humidity stability. It can be applied to biological penetration detection and potential marine life engineering applications.

**Author Contributions:** Conceptualization, Y.Z.; methodology, Y.Z.; formal analysis, Y.Z. and S.Z.; writing—original draft preparation, Y.Z.; writing—review and editing, Y.Z., S.Z., H.G., D.X., Z.H. and Z.G.; supervision, J.S. and C.L.; project administration, J.S. and C.L. All authors have read and agreed to the published version of the manuscript.

**Funding:** This work is supported by the Finance Science and Technology Project of Hainan Province (ZDKJ2020009) and the Hainan Provincial Natural Science Foundation of China (2019RC054).

**Institutional Review Board Statement:** Not applicable.

**Informed Consent Statement:** Not applicable.

**Data Availability Statement:** Research data presented in this study are available on request from the corresponding author.

**Acknowledgments:** Shen provides materials used for experiments.

**Conflicts of Interest:** The authors declare no conflict of interest.

## References

1. Gao, H.; Jiang, Y.; Zhang, L.; Cui, Y.; Jiang, J.; Jiang, L. Antiresonant mechanism based self-temperature-calibrated fiber optic Fabry–Perot gas pressure sensors. *Opt. Express* **2019**, *27*, 22181–22189. [[CrossRef](#)] [[PubMed](#)]
2. Li, Z.; Zhang, Y.-X.; Zhang, W.-G.; Kong, L.-X.; Yan, T.-Y.; Geng, P.-C.; Wang, B. High-Sensitivity Gas Pressure Fabry–Perot Fiber Probe With Micro-Channel Based on Vernier Effect. *J. Light. Technol.* **2019**, *37*, 3444–3451. [[CrossRef](#)]
3. Xu, F.; Ren, D.; Shi, X.; Li, C.; Lu, W.; Lu, L.; Lu, L.; Yu, B. High-sensitivity Fabry–Perot interferometric pressure sensor based on a nanothick silver diaphragm. *Opt. Lett.* **2012**, *37*, 133–135. [[CrossRef](#)] [[PubMed](#)]
4. Quan, M.; Tian, J.; Yao, Y. Ultra-high sensitivity Fabry–Perot interferometer gas refractive index fiber sensor based on photonic crystal fiber and Vernier effect. *Opt. Lett.* **2015**, *40*, 4891–4894. [[CrossRef](#)] [[PubMed](#)]
5. FFu, H.Y.; Tam, H.Y.; Shao, L.; Dong, X.; Wai, A.; Lu, C.; Khijwania, S.K. Pressure sensor realized with polarization-maintaining photonic crystal fiber-based Sagnac interferometer. *Appl. Opt.* **2008**, *47*, 2835–2839. [[CrossRef](#)]
6. Martynkien, T.; Statkiewicz-Barabach, G.; Olszewski, J.; Wojcik, J.; Mergo, P.; Geernaert, T.; Sonnenfeld, C.; Anuszkiewicz, A.; Szczurowski, M.K.; Tarnowski, K.; et al. Highly birefringent microstructured fibers with enhanced sensitivity to hydrostatic pressure. *Opt. Express* **2010**, *18*, 15113–15121. [[CrossRef](#)] [[PubMed](#)]
7. Li, Z.; Jia, P.; Fang, G.; Liang, H.; Liang, T.; Liu, W.; Xiong, J. Microbubble-based fiber-optic Fabry–Perot pressure sensor for high-temperature application. *Appl. Opt.* **2018**, *57*, 1738–1743. [[CrossRef](#)]
8. Ge, Y.; Cai, K.; Wang, T.; Zhang, J. MEMS pressure sensor based on optical Fabry–Perot interference. *Optik* **2018**, *165*, 35–40. [[CrossRef](#)]
9. Domingues, M.F.; Rodriguez, C.A.; Martins, J.; Tavares, C.; Marques, C.; Alberto, N.; André, P.; Antunes, P. Cost-effective optical fiber pressure sensor based on intrinsic Fabry–Perot interferometric micro-cavities—ScienceDirect. *Opt. Fiber Technol.* **2018**, *42*, 56–62. [[CrossRef](#)]
10. Zhao, Y.; Chen, M.-Q.; Xia, F.; Lv, R.-Q. Small In-fiber Fabry–Perot low-frequency acoustic pressure sensor with PDMS diaphragm embedded in hollow-core fiber. *Sens. Actuators A Phys.* **2018**, *270*, 162–169. [[CrossRef](#)]
11. Gao, H.; Wang, J.; Shen, J.; Zhang, S.; Xu, D.; Zhang, Y.; Li, C. Study of the Vernier Effect Based on the Fabry–Perot Interferometer: Methodology and Application. *Photonics* **2021**, *8*, 304. [[CrossRef](#)]
12. Liao, C.; Liu, S.; Xu, L.; Wang, C.; Wang, Y.; Li, Z.; Wang, Q.; Wang, D.N. Sub-micron silica diaphragm-based fiber-tip Fabry–Perot interferometer for pressure measurement. *Opt. Lett.* **2014**, *39*, 2827–2830. [[CrossRef](#)]
13. Yeo, T.; Sun, T.; Grattan, K. Fibre-optic sensor technologies for humidity and moisture measurement. *Sens. Actuators A Phys.* **2008**, *144*, 280–295. [[CrossRef](#)]
14. Coulet, P.R.; Blum, L.J.; Gautier, S.M. Luminescence-based fibre-optic probes. *Sens. Actuators B Chem.* **1993**, *11*, 57–61. [[CrossRef](#)]
15. He, L.; Pagneux, Q.; Larroulet, I.; Serrano, A.Y.; Pesquera, A.; Zurutuza, A.; Mandler, D.; Boukherroub, R.; Szunerits, S. Label-free femtomolar cancer biomarker detection in human serum using graphene-coated surface plasmon resonance chips. *Biosens. Bioelectron.* **2017**, *89*, 606–611. [[CrossRef](#)] [[PubMed](#)]
16. Min, R.; Liu, Z.; Pereira, L.; Yang, C.; Sui, Q.; Marques, C. Optical fiber sensing for marine environment and marine structural health monitoring: A review. *Opt. Laser Technol.* **2021**, *140*, 107082. [[CrossRef](#)]
17. Chen, M.Q.; Zhao, Y.; Xia, F.; Peng, Y.; Tong, R.J. High sensitivity temperature sensor based on fiber Air-Microbubble Fabry–Perot interferometer with PDMS-filled hollow-core fiber. *Sens. Actuators A Phys.* **2018**, *275*, 60–66. [[CrossRef](#)]
18. Beheim, G.; Fritsch, K.; Poorman, R.N. Fiber-linked interferometric pressure sensor. *Rev. Sci. Instrum.* **1987**, *58*, 1655–1659. [[CrossRef](#)]

19. Liu, S.; Yang, K.; Wang, Y.; Qu, J.; Liao, C.; He, J.; Li, Z.; Yin, G.; Sun, B.; Zhou, J.; et al. High-sensitivity strain sensor based on in-fiber rectangular air bubble. *Sci. Rep.* **2015**, *5*, 7624. [[CrossRef](#)] [[PubMed](#)]
20. Donlagic, D.; Cibula, E. All-fiber high-sensitivity pressure sensor with SiO<sub>2</sub> diaphragm. *Opt. Lett.* **2005**, *30*, 2071–2073. [[CrossRef](#)]
21. Xu, B.; Wang, C.; Wang, D.N.; Liu, Y.; Li, Y.J.O.E. Fiber-tip gas pressure sensor based on dual capillaries. *Opt. Express* **2015**, *23*, 23484–23492. [[CrossRef](#)] [[PubMed](#)]
22. Wang, X.; Xu, J.; Zhu, Y.; Cooper, K.L.; Wang, A. All-fused-silica miniature optical fiber tip pressure sensor. *Opt. Lett.* **2006**, *31*, 885–887. [[CrossRef](#)] [[PubMed](#)]
23. Wang, T.; Ge, Y.; Ni, H.; Chang, J.; Zhang, J.; Ke, W. Miniature fiber pressure sensor based on an in-fiber confocal cavity. *Optik* **2018**, *171*, 869–875. [[CrossRef](#)]
24. Oliveira, R.F.; Billo, L.; Nogueira, R.; Rocha, A.M.M. Adhesive Based Fabry-Pérot Hydrostatic Pressure Sensor With Improved and Controlled Sensitivity. *J. Lightwave Technol.* **2019**, *37*, 1909–1915. [[CrossRef](#)]
25. Luo, C.; Liu, X.; Liu, J.; Shen, J.; Li, H.; Zhang, S.; Hu, J.; Zhang, Q.; Wang, G.; Huang, M. An Optimized PDMS Thin Film Immersed Fabry-Perot Fiber Optic Pressure Sensor for Sensitivity Enhancement. *Coatings* **2019**, *9*, 290. [[CrossRef](#)]
26. Zhang, S.; Shao, Z.; Liu, J.; Zong, M.; Shen, J.; Gao, H.; Wang, G.; Huang, M. An Optical Fiber Fabry—Perot Pressure Sensor with Optimized Thin Microbubble Film Shaping for Sensitivity Enhancement. *Coatings* **2020**, *10*, 358. [[CrossRef](#)]
27. Wei, X.; Song, X.; Li, C.; Hou, L.; Li, Z.; Li, Y.; Ran, L. Optical Fiber Gas Pressure Sensor Based on Polydimethylsiloxane Microcavity. *J. Lightwave Technol.* **2021**, *39*, 2988–2993. [[CrossRef](#)]
28. Rao, Y.-J.; Deng, M.; Duan, D.; Zhu, T. In-line fiber Fabry-Perot refractive-index tip sensor based on endlessly photonic crystal fiber. *Sens. Actuators A Phys.* **2008**, *148*, 33–38. [[CrossRef](#)]
29. Osório, J.H.; Chesini, G.; Serrão, V.A.; Franco, M.A.R.; Cordeiro, C.M.B. Simplifying the design of microstructured optical fibre pressure sensors. *Sci. Rep.* **2017**, *7*, 1–9. [[CrossRef](#)]
30. Hou, L.; Zhao, C.; Xu, B.; Mao, B.; Shen, C.; Wang, D.N. Highly sensitive PDMS-filled Fabry-Perot interferometer temperature sensor based on the Vernier effect. *Appl. Opt.* **2019**, *58*, 4858–4865. [[CrossRef](#)] [[PubMed](#)]
31. Zhao, C.; Hou, L.; Kang, J.; Mao, B.; Shen, C.; Jin, S. High-sensitivity hydraulic pressure sensor based on Fabry-Perot interferometer filled with polydimethylsiloxane film. *Rev. Sci. Instrum.* **2019**, *90*, 095002. [[CrossRef](#)] [[PubMed](#)]
32. Zhe, Z.; He, J.; Liao, C.; Jian, T.; Wang, Y. A novel fabrication method of fiber-tip Fabry-Perot interferometer for high-sensitivity gas-pressure measurements. In Proceedings of the 2017 16th International Conference on Optical Communications and Networks (ICOON), Wuzhen, China, 7–10 August 2017.
33. Liu, S.; Wang, Y.; Liao, C.; He, J.; Fu, C.; Yang, K.; Bai, Z.; Zhang, F. Nano silica diaphragm in-fiber cavity for gas pressure measurement. *Sci. Rep.* **2017**, *7*, 1–9. [[CrossRef](#)]
34. Ma, J.; Ju, J.; Jin, L.; Jin, W. A Compact Fiber-Tip Micro-Cavity Sensor for High-Pressure Measurement. *IEEE Photonics Technol. Lett.* **2011**, *23*, 1561–1563. [[CrossRef](#)]
35. Guo, X.; Zhou, J.; Du, C.; Wang, X. Highly Sensitive Miniature All-Silica Fiber Tip Fabry–Perot Pressure Sensor. *IEEE Photonics Technol. Lett.* **2019**, *31*, 689–692. [[CrossRef](#)]